Energy Transfer Kinetics of N2(X1 ,v) and SiH4†

ARTICLE *in* THE JOURNAL OF PHYSICAL CHEMISTRY A · AUGUST 2002

Impact Factor: 2.69 · DOI: 10.1021/jp020005d

Energy Transfer Kinetics of $N_2(X^1\Sigma_u^+,v)$ and SiH_4[†]

Lawrence G. Piper[‡]

Physical Sciences Inc., 20 New England Business Center, Andover, Massachusetts 01810

Received: January 8, 2002; In Final Form: June 17, 2002

We have studied the kinetics of $N_2(X,v)$ with silane. These experiments were done in a discharge-flow reactor and used $N_2(X,v)$ diagnostics employing metastable energy transfer reactions. To investigate vibrational levels greater than five, and up to at least thirteen, we analyze $N_2(B^3\Pi g,v'\leq 12)$ fluorescence excited in the interaction between metastable $N_2(A^3\Sigma_u^+)$ and $N_2(X^1\Sigma_g^+,v)$. N_2^+ $(B^2\Sigma_g^+,v'=0-8)$ fluorescence, excited when metastable helium atoms collide with $N_2(X,v)$, diagnoses vibrational levels between one and six. The rate coefficients for quenching vibrationally excited nitrogen by silane range from 1×10^{-13} to 6×10^{-13} cm^3 molecule^{-1} s^{-1}, being higher for the higher vibrational levels. Observations at 4500 nm show that at least one channel for the $N_2(X,v)$ quenching process involves excitation of $SiH_4(\nu_3)$. Comparison of the relative excitation rate of $SiH_4(\nu_3)$ with that for $N_2O(\nu_3)$ excitation when N_2O is added to the reactor, however, indicates that at most 15% of the $N_2(X,v)$ quenching events result in ν_3 excitation. Presumably the rest of the energy is absorbed by other vibrational modes.

1. Introduction

Understanding the role of molecular nitrogen in a chemical system requires knowledge of the reactivity of the various states of nitrogen which might be important. To study a state's reactivity, one needs a diagnostic of that state. In the case of vibrationally excited nitrogen in its ground electronic state, this proves to be a difficult task. Unlike most other diatomic molecules, nitrogen does not have a dipole moment, and so is infrared inactive. In addition, nitrogen has no readily accessible higher lying electronic states so that absorption or laser excitation studies are difficult to implement. Thus much information on the kinetics of vibrationally excited nitrogen in its ground electronic state has employed either complex diagnostics or diagnostics which were incapable of providing much by way of state specificity. That is, some distinction could be made between vibrationally excited and unexcited nitrogen, but very little could be said regarding whether higher levels differed in reactivity compared to the lower ones.

For example, Morgan and Schiff[1] used a catalytic probe to detect $N_2(v)$ in an afterglow from which they had first removed atomic nitrogen, a species that would also have released heat to the probe. McNeal et al.[2−4] took advantage of the fact that the photoionization threshold would be lower for $N_2(v=1)$ than it would be for $N_2(v=0)$ to make kinetic measurements on $N_2(v)$. Starr and Shaw[5] monitored fluorescence from atomic potassium that had been excited by energy transfer from $N_2(v>9)$ to measure the kinetics of $N_2(v)$ quenching by N_2 and CO_2. In all of these cases the diagnostics were incapable of providing any information on the energy transfer probabilities from different $N_2(v)$ vibrational levels, although in the case of the Starr and Shaw work, the $N_2(v)$ monitored was in higher vibrational levels. In the other two cases mentioned, it was only for the lowest excited vibrational level.

De Benedictis et al.[6] combined observations of infrared fluorescence from CO that had been pumped by $N_2(v)$ with a complex modeling scheme to infer $N_2(v)$ vibrational distributions in a discharge. Mutel et al.[7] used a laser Raman probe to deduce $N_2(v)$ distributions in a discharge, and more recently several groups have worked toward developing a coherent anti Stokes Raman (CARS) diagnostic for $N_2(v)$ in discharges and discharge afterglows.[8,9]

All of these efforts either have been limited in their ability to diagnose $N_2(v)$ in more than a single vibrational level or else have been limited to cases in which the $N_2(v)$ number densities were relatively large. Though this latter condition is often adequate for diagnostic studies of concentrations inside a discharge, the lack of sensitivity makes it difficult to carry out kinetic studies that will be free from secondary reaction effects.

A number of years ago we developed several diagnostics for vibrationally excited nitrogen in its ground electronic state.[10] These included laser-induced fluorescence in the far ultraviolet using the metastable N_2 $(a^1\Pi_g)$ state, multiphoton ionization, and two diagnostics that relied on metastable species to excite visible nitrogen fluorescence. For the purposes of kinetic studies, the two metastable-transfer diagnostics were most sensitive and easiest to implement. We used one of them,[11,12] the energy transfer reaction between metastable $N_2(A^3\Sigma_u^+)$ and $N_2(X^1\Sigma_g^+)$, to explore briefly the quenching of vibrationally excited nitrogen in levels between about 5 and 13 by nine different molecules, including O_2, N_2O, and CO_2.[13]

In this paper, we use that diagnostic and another, the Penning ionization of $N_2(X^1\Sigma_g^+,v)$ by metastable He*$(2\ ^3S)$,[14−17] to explore in some detail the quenching of vibrationally excited nitrogen by silane,

$$N_2(X^1\Sigma_g^+,v) + SiH_4 \rightarrow N_2(X^1\Sigma_g^+,v-1) + SiH_4(\nu_3,\nu_1) \quad (1)$$

The two diagnostics are complementary. The one using metastable helium provides information on the lower vibrational levels, $v'' = 0-6$, whereas that using the metastable nitrogen diagnoses higher vibrational levels, $v'' \sim 5-13$. We also observed infrared emission from vibrationally excited silane,

[†] Part of the special issue "Donald Setser Festschrift".

[‡] Tel: 978-689-0003. E-mail: piper@psicorp.com. Fax: 978-689-3232.

10.1021/jp020005d CCC: $22.00
Published on Web 08/08/2002

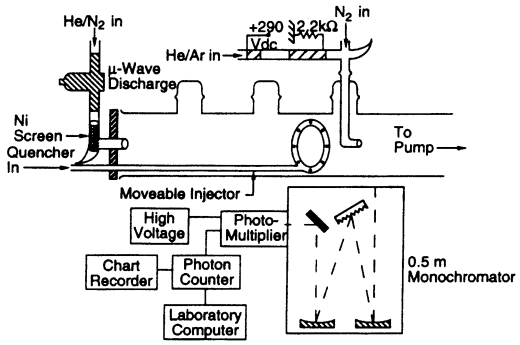

Figure 1. Discharge flow reactor for studying the kinetics of reactions involving $N_2(X,v)$.

showing that this excitation is indeed one product from the energy transfer reaction.

The interest in this particular system stems from the use of remote plasma enhanced chemical vapor deposition (RPECVD) to make silicon nitride films. In one variant of that technique, silane is added to the effluents of a discharge containing nitrogen, or nitrogen/rare gas mixtures.[18−22] To model such a system properly, one needs kinetic information on vibrationally excited nitrogen, especially because first exciting vibrational modes in silane might be one means of making the reaction between atomic nitrogen and silane exoergic.[23] Our technique is general, however, and can readily be applied to study vibrational energy transfer reactions important in other systems, such as discharges, gas lasers, and the disturbed upper atmosphere.

The following sections provide first a description of the general apparatus and procedures. Then we discuss in depth the two energy transfer diagnostics and show how they can be applied to studying vibrational quenching of nitrogen in all levels between $v'' = 1$ and $v'' \sim 13$. We next discuss several different approaches we have applied to derive kinetic information in this system. Using the above two mentioned diagnostics, we obtain quenching rate coefficients for the various vibrational levels, and show that our results are consistent with a single-quantum transfer mechanism. In addition, observing variations in the infrared fluorescence from $SiH_4(\nu_3)$ as a function of time and concentration provides some confirmation of the measured quenching rate coefficients and allows us to estimate the efficiency with which $SiH_4(\nu_3)$ fluorescence is excited by $N_2(X,v)$.

2. Experimental Section

The experiments were all done in a discharge-flow reactor. Different configurations were used depending upon the effects being studied. The bulk of the experiments, designed to measure rate coefficients for $N_2(X,v)$ removal by SiH_4, used the apparatus shown schematically in Figure 1. It consists of a 4.6-cm i.d. quartz tube, 50 cm long. $N_2(X,v)$ is injected into the upstream end of the reactor and is detected at the downstream end by monitoring fluorescence excited by the interaction of $N_2(X,v)$ with either $N_2(A)$ or $He(2^3S)$. A loop injector that can be moved along the length of the reactor mixes silane with $N_2(X,v)$. The loop injector directs the silane both toward the center of the flow reactor and also toward its periphery. This bidirectional injection coupled with the fact that the bulk of the gas in the flow tube is helium serves to provide rapid uniform mixing. Chemiluminescent observations in this system have shown mixing to be complete by the time gas has flowed 2−3 cm downstream from the injector. The flow reactor was pumped by a roots blower/forepump combination capable of producing flow velocities of 5×10^3 cm s^{-1} at a pressure of 1 Torr. Generally, much more modest flow velocities were required and the flow reactor access to the pump was throttled by a downstream butterfly valve.

$N_2(X,v)$ is prepared in a microwave discharge through a mixture of nitrogen dilute in helium. The effluents of the discharged mixture then pass through a nickel screen prior to their entry into the flow reactor. The screen removes the atoms and ions and deactivates the electronically excited metastables produced in the discharge but has relatively little effect on vibrationally excited N_2.[10,11] Our previous observations[24] indicate that the Ni screen reduces N atom number densities about a factor of 50, to a level of about 1×10^{11} cm^3 molecule^{-1} s^{-1}. This reduction is, of course, dependent to some extent upon the screen mesh and contact time between the discharge effluents and the screen. In our experiments the screen is about 24 mesh and consists of two coaxial cylinders about 5 cm long inserted into the 12.7 mm o.d. discharge tube downstream from the discharge. They cover the opening in the side of the discharge tube through which the effluents must pass to enter the flow reactor.

Metastable $He(2^3S)$ or $N_2(A^3\Sigma_u^+)$ enter the flow reactor through a 10 cm o.d. hook-shaped injector inserted into the flow reactor at its downstream end. The metastables are generated in the upstream end of the injector and emanate from the injector along the flow reactor axis. A hollow cathode, dc discharge, biased at 290 V dc, generates $He(2^3S)$ if the injector flow is pure helium, or metastable $Ar(^3P_{0,2})$ if a few percent argon is added to the helium flow. The metastable argon is used to produce the $N_2(A)$ metastables by excitation transfer.[25] In this case, nitrogen is added in the injector just downstream from the discharge cathode. The lack of emission from $N_2^+(C)$ or $N_2^+(B,v\geq 2)$ when the He metastables are added to cold N_2 shows that both He^+ and He_2^+ are absent from the flow of metastables entering the flow reactor.[26]

The flame emanating from this injector when the metastables are mixed with the main flow appears to be roughly the diameter of the injector orifice, 10 mm, and is relatively uniform and intense for the first centimeter downstream from the injector. It then fans out and fades as the metastables are consumed and as they diffuse toward the walls of the flow reactor. The shape of the metastable flame is not relevant to the kinetic observations because all measurements are based on relative intensities under constant conditions of pressure, flow rate, silane concentration, and viewing location, but with differing mixing times for the silane and the $N_2(v)$. This point will become more apparent below when we describe the kinetic analysis.

Gas flow rates are measured by electronic mass flow meters, or in a few instances by rotameters, that have been calibrated by measuring the rates of pressure increase as a function of time when gases flow into a calibrated volume. Because some of our initial results were puzzling, the mass flow meters were extensively recalibrated. The only significant change from this procedure was that the SiH_4 calibration was about 15% less than we had anticipated on the basis of the flow meter calibration with argon and the standard correction procedure involving the ratio of gas specific heats. Capacitance manometers measured the flow reactor pressures.

A 0.5 m monochromator, sensitive to radiation between 200 and 900 nm, detected emission in the flow reactor. The emission is observed directly through the wall of the flow tube using an imaging system that effectively projects the image of the slit across the flow tube. That is, the field of view is essentially a

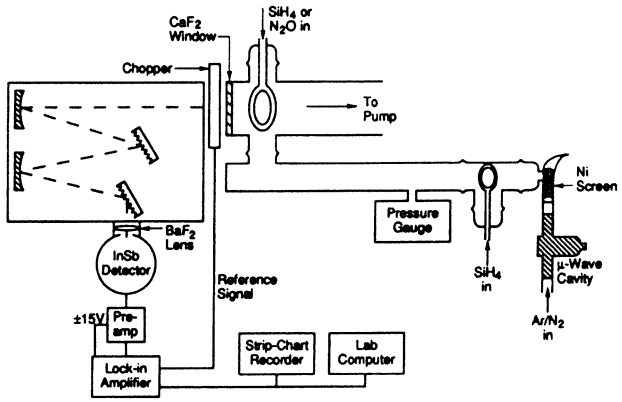

Figure 2. Schematic of apparatus for observing $SiH_4(\nu_3)$ infrared emission.

slice across the diameter of the flow tube that is about 10 mm in height and a few millimeters in width (along the flow tube axis). The monochromator had a 1200 groove mm^{-1} grating blazed at 250 nm and a thermoelectrically cooled photomultiplier. Signals from the photomultiplier were processed by either a photon-counting rate meter or a picoammeter. Their outputs were recorded by a strip-chart recorder and stored digitally by a lab computer system. A least-squares, spectral fitting procedure, described in some detail previously, determined band intensities from the spectra:[27] the N_2 first-negative bands, N_2^+ ($B^2\Sigma^+-X^2\Sigma^+$) between 350 and 500 nm, from the $He^*(2^3S)/N_2(X,v\leq 6)$ interaction; the N_2 first-positive bands, $N_2(B^3\Pi_g-A^3\Sigma_u^+)$ between 560 and 900 nm, from the $N_2(A^3\Sigma_u^+)/N_2(X,v\geq 5)$ interaction; and the N_2 Vegard−Kaplan bands, $N_2(A^3\Sigma_u^+-X^1\Sigma_g^+)$ between 250 and 400 nm, diagnostic of $N_2(A)$ number densities.

Another set of experiments used the apparatus shown schematically in Figure 2. These experiments were designed to monitor infrared fluorescence from SiH_4 or N_2O excited by vibration−vibration exchange from $N_2(X,v)$. For these experiments a 5 cm i.d. flow tube was configured to allow spectral observations along the axis of the flow reactor. The upstream end of the flow reactor was sealed with a CaF_2 window and placed directly in front of the monochromator slit. The effective field of view was about 32 cm long. Generally, the $N_2(X,v)$ entered directly in front of the window, normal to the axis of the field of view. Silane, or in some cases nitrous oxide, was added through a loop injector situated directly in front of the window.

The infrared spectral observations were made between 2000 and 5000 nm using the 0.5 m monochromator equipped with a 150 groove mm^{-1} grating blazed at 3000 nm and a liquid nitrogen cooled InSb detector. Light from the observation region was chopped prior to entering the monochromator and signals from the detector were processed with a phase-sensitive amplifier. The output from the lock-in amplifier was recorded by a strip-chart recorder and, in addition, stored digitally in a computer file.

3. Energy-Transfer Based Diagnostics of $N_2(X,v)$

We have developed techniques for determining number densities of vibrationally excited nitrogen in vibrational levels up through about fifteen.[10−12,17] Two different methods are used to probe different ranges of vibrational excitation. The first, which gives absolute $N_2(X,v)$ number densities for vibrational levels up through about six, involves measuring the vibrational distribution of the nitrogen first-negative bands when they are excited in the Penning-ionization reaction between metastable helium atoms and $N_2(X,v)$,

$$He^*(2^3S) + N_2(X,v) \rightarrow He(^1S) + N_2^+(B,v) \qquad (2)$$

The ground-electronic-state vibrational distribution of nitrogen can be deduced from the $N_2^+(B)$ vibrational distribution and the Franck−Condon factors that connect the ground electronic state of the neutral molecule to the electronically excited state of the molecular ion (vide infra).[10,17]

The second $N_2(X,v)$ diagnostic gives semiquantitative estimates of $N_2(X,v)$ number densities for vibrational levels greater than 4 (about 5−13).[11,12] Metastable nitrogen molecules, $N_2(A^3\Sigma_u^+)$, excite $N_2(X,v\sim 5-13)$ to $N_2(B,v\leq 12)$ quite efficiently,

$$N_2(A^3\Sigma_u^+) + N_2(X,v) \rightarrow N_2(X) + N_2(B^3\Pi_g,v\leq 12) \quad (3)$$

where $k_3 \sim 4 \times 10^{-11}$ cm^3 $molecules^{-1}$ s^{-1}. Measurements of the intensity and vibrational distribution of the $N_2(B)$ fluorescence in the presence of known amounts of $N_2(A)$ will give the number densities of these highly excited levels of $N_2(X,v)$ to within factors of 2−3. Relative variations in $N_2(X,v)$ number densities can be determined to within about 20%.

We have employed this second $N_2(X,v)$ diagnostic to determine rate coefficients for vibrational energy transfer from $N_2(X,v)$ to a number of other molecules.[13] The technique involves comparing the $N_2(B)$ intensities from $N_2(A)$ excitation of $N_2(X,v)$ between conditions under which the mixing time of the quencher and the vibrationally excited nitrogen is quite short, 2−3 ms, and conditions under which the contact time is much longer, 20−40 ms. This approach allows one to distinguish between reductions in $N_2(B)$ intensity caused by electronic quenching of $N_2(B)$ from those resulting from a reduction in the $N_2(X,v)$ number density. We describe this analysis in more detail below.

3.1. Penning Ionization. Our Penning-Ionization diagnostic for vibrationally excited nitrogen in discharge afterglows follows along the lines of the pioneering work of Schmeltekopf et al.[14] and Young and Horn.[15,16] Mixing metastable helium atoms with a flow of molecular nitrogen results in strong emission of the nitrogen first-negative system, $N_2^+(B^2\Sigma_u^+-X^2\Sigma_g^+)$. Because the Penning-ionization process follows a Franck−Condon excitation pathway, the vibrational distribution in the neutral, ground state will determine the distribution observed in the upper, ionic state. One problem with this approach is that care must be taken not to have any He^+ or He_2^+ in the flow of metastable helium. Both of those species also excite $N_2^+(B)$ quite strongly in charge-transfer reactions, but with an $N_2^+(B)$ vibrational distribution that is decidedly non-Franck−Condon.[26] We took care to ensure the absence of ions in our system, as mentioned above.

The rate of Penning-ionization between metastable helium atoms and molecular nitrogen is proportional to the Franck−Condon factors that connect the $N_2^+(B)$ and $N_2(X)$ states. One can calculate the vibrational distribution in the final state, therefore, knowing only the vibrational distribution in the lower state and the Franck−Condon factors that couple the two states. Thus,

$$N_{v'} \propto \sum_{v''} N_{v''} q_{v'v} \qquad (4)$$

where v' and v'' represent the vibrational levels of the upper and lower states, respectively, and $q_{v'v''}$ is the Franck−Condon factor coupling them. We have calculated a comprehensive set

of Franck−Condon factors for $N_2^+(B)-N_2(X)$ transitions and have tabulated them elsewhere.[28]

We determine relative $N_2(X,v)$ distributions by finding the model distribution that can be used in eq 4 to predict $N_2^+(B)$ vibrational distributions that are most like those observed experimentally. The $N_2(X,v)$ vibrational distributions usually follow a modified Treanor[29−31] model, which simplifies the fitting process. We do have fitting procedures, however, to determine populations for cases for which the Treanor model is inapplicable.[10]

The modified Treanor distribution has been outlined by Caledonia and Center,[30] and Dilonardo and Capitelli.[31] For low vibrational levels the distribution is that given by Treanor et al.:[29]

$$\frac{N_{v''}}{N_{v=0}} = \exp\left(-v''\left[\frac{1.4388(\omega_e - 2\omega_e x_e)}{\Theta_1} - (v'' - 1)\frac{1.4388\omega_e x_e}{T}\right]\right) \quad (5)$$

where Θ_1 is the Boltzmann vibrational temperature referenced to $v'' = 1$, T is the ambient gas translational temperature, and ω_e and $\omega_e x_e$ are spectroscopic constants in units of cm^{-1}. The Boltzmann vibrational temperature is given by

$$\Theta_1 = -\frac{\omega_e - 2\omega_e x_e}{k \ln(N_{v''=1}/N_{v''=0})} \quad (6)$$

where k is Boltzmann's constant.

This distribution goes through a minimum, called the Treanor minimum, at v^*, given by

$$v^* = \frac{T(\omega_e - 2\omega_e x_e)}{2\omega_e x_e \Theta_1} + 0.5 \quad (7)$$

For vibrational levels above the Treanor minimum, the Product vN_v is essentially constant.[30] The resulting distribution for $v > v^*$ is

$$\frac{N_{v''}}{N_{v''=0}} = \frac{(v^* - 1)\exp(-1.4388(v^{*2} - 1)\omega_e x_e/T)}{v''} \quad (8)$$

where the various parameters in eq 8 are determined by requiring the two distributions, i.e., eqs 5 and 8, be equal at v'' and $v^* - 1$. Rather than use an explicit Θ_1 value, we base our distributions on an effective Θ_1 that best fits all the data points.

Fitting the Penning-ionization spectra to a ground-state vibrational model, as just described, gives only the relative distribution among ground-state vibrational levels. We place this relative distribution on an absolute basis, however, by determining the absolute number density of $N_2(X,v''=0)$. This is accomplished by noting changes in intensity of $N_2^+(B,v'=0,1)$ when the $N_2(X,v)$ producing discharge is struck relative to the intensities when the discharge is off. We know, of course, the absolute $N_2(X,v''=0)$ number density when the discharge is off from the relative flow rates of the various gases in the system and the absolute pressure.

3.2. $N_2(A)$ Energy Transfer. The Penning-ionization diagnostic is inadequate for studies on $N_2(X,v''\gtrsim 6)$, as discussed earlier. To overcome this problem we developed a semiquantitative technique for determining number densities of $N_2(X,v''\geq 5)$. Our diagnostic method for monitoring $N_2(X,v''\geq 5)$ is based upon measuring nitrogen first-positive emission intensities excited in the reaction between $N_2(A)$ and $N_2(X,v'')$.[11,12] These intensities are directly proportional to $N_2(X,v'')$ number densities. The observed intensities must be corrected for any quenching of the first-positive emission before they can be related to $N_2(X,v'')$ number densities.

The intensity of the N_2 first-positive emission is given by

$$I = k_r[N_2(B)] = \frac{k_3 N_2(X,v'')[N_2(A)]}{1 + \sum_i \frac{k_{Q_i}[Q_i]}{k_r}} \quad (9)$$

where k_{Q_i} is the rate coefficient for $N_2(B)$ quenching by quenchers Q_i and k_r is the $N_2(B)$ radiative decay rate.[27] The buffer gas pressure, primarily helium, is 1 Torr. This minimizes quenching by the bath gas species in the flow tube.[32] Rearranging eq 9 gives

$$[N_2(X,v)] = \frac{k_r[N_2(B)]}{k_3[N_2(A)]}\left\{1 + \sum_i \frac{k_{Q_i}[Q_i]}{k_r}\right\} \quad (10)$$

whereas determining absolute values for $[N_2(A)]$ or $[N_2(B)]$ is difficult and therefore quite uncertain, measuring the ratio of these two number densities accurately is straightforward because only relative sensitivities of the detection system at the various wavelengths are required.

Although primarily a global monitor of $N_2(X,v'')$, this diagnostic does provide some state specificity. The higher vibronic levels of $N_2(B)$ are accessible only from $N_2(X,v'')$ vibrational levels at the high end of the diagnostic range. For example, $N_2(B,v'=10)$ can be excited only from $N_2(X,v''\geq 12)$. Thus, we can track the varying behavior of $N_2(X,v''\geq 12)$ by measuring $N_2(B,v=10)$ intensities. Similar arguments hold for other $N_2(X,v'')$ and $N_2(B,v)$.

4. $N_2(X,v)$ Quenching by SiH_4

4.1. Experimental Approach. Because our diagnostic techniques involve adding metastables to the flow reactor and observing the fluorescence excited when the metastable interacts with $N_2(X,v)$, we need to separate diminutions in the observed fluorescence caused by fluorescence or metastable quenching from the diminutions resulting from removal of $N_2(X,v)$ from the reactor. We separate these effects by varying the mixing time between the $N_2(X,v)$ and the SiH_4 over a wide range.

When quencher is injected immediately behind the $N_2(A)$ (or He*) inlet, the number density of $N_2(X,v'')$ remains essentially unchanged. This is because vibrational quenching is a relatively slow process ($k_v \sim 10^{-13}$ cm^3 $molecule^{-1}$ s^{-1}) and reagents are mixed for too short of time (2 ms) to effect significant quenching. Any diminution in the first-positive (negative) emission, therefore, results from quenching of $N_2(B)$ ($N_2^+(B)$), or perhaps $N_2(A)$ (He*). Injecting the reagent at the upstream end of the flow reactor allows adequate time (∼10−30 ms) for the $N_2(X,v'')$ to be quenched unless the quenching rate coefficients are exceedingly small. Any difference in diminution of the first-positive (negative) emission with the injector in the upstream position as compared to the downstream position can be attributed to quenching of $N_2(X,v'')$ by the added reagent.

Figure 3 illustrates these concepts. It shows a portion of the spectrum of $N_2(B-A)$ emission, excited by the reaction between $N_2(A)$ and $N_2(X,v)$, in the absence of any added quencher and in the presence of a fixed concentration of SiH_4 at a small mixing time, and at one 21.7 ms greater. Adding the SiH_4 at

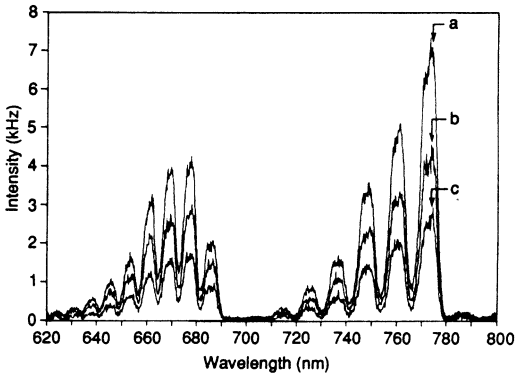

Figure 3. Variation in the $N_2(B-A)$ intensity excited in the $N_2(A) + N_2(X,v)$ reaction, as a function of reaction time and SiH_4 number density. Conditions in the order of decreasing intensity: (a) $[SiH_4] = 0$, $\Delta t = 0$ ms; (b) $[SiH_4] = 2.3 \times 10^{13}$ molecules cm^{-3}, $\Delta t = 0$ ms; (c) $[SiH_4] = 2.3 \times 10^{13}$ molecules cm^{-3}, $\Delta t = 21.7$ ms.

the short time drops the $N_2(B-A)$ emission about a factor of 1.6. When the mixing time is increased by 21.7 ms, the first-positive emission intensity diminishes almost another factor of 1.6. We can estimate rate coefficients for $N_2(X,v)$ and $N_2(B,v)$ quenching by SiH_4 from data such as these as shown below.

In the absence of added quencher, the intensity of the N_2 first-positive emission is given by[11,12]

$$I_o = k_r[N_2(B)] = k_3[N_2(X,v'')][N_2(A)] \tag{11}$$

For global measurements, k_r, the radiative decay rate of the $N_2(B)$,[27] is about 1.5×10^5 s^{-1}. The experiments use a helium bath-gas at pressures of about 1 Torr. This reduces quenching in the flow tube to less than a 20% effect.[32] As a result we neglect bath-gas quenching in eq 11.

When the quencher is introduced into the flow reactor with the injector in the downstream position, that is, short interaction times where $N_2(X,v)$ removal is negligible, the first-positive emission intensity is given by

$$I_o = k_r[N_2(B)] = \frac{k_3[N_2(A)][N_2(X,v'')]}{1 + \dfrac{k_Q[Q]}{k_r}} \tag{12}$$

where k_Q is the rate coefficient for $N_2(B)$ quenching by SiH_4. $N_2(A)$ number densities are also measured under each set of conditions to correct any quenching of the $N_2(A)$. Taking the ratio of the first-positive intensity in the absence of quencher to that in the presence of quencher gives the classical Stern−Volmer formula[33] for electronic quenching, viz.,

$$\Gamma = \frac{I_o/[N_2A]_o}{I/[N_2A]} = 1 + k_Q[Q]/k_r \tag{13}$$

where the subscript "o" refers to conditions in the absence of added quencher. The rate coefficient for $N_2(B)$ quenching for data taken with the injector in the downstream position is

$$k_Q = \frac{k_r}{[Q]}\{\Gamma - 1\} \tag{14}$$

With the injector in the upstream position, the $N_2(X,v'')$ is also quenched and the first-positive emission intensity is described by

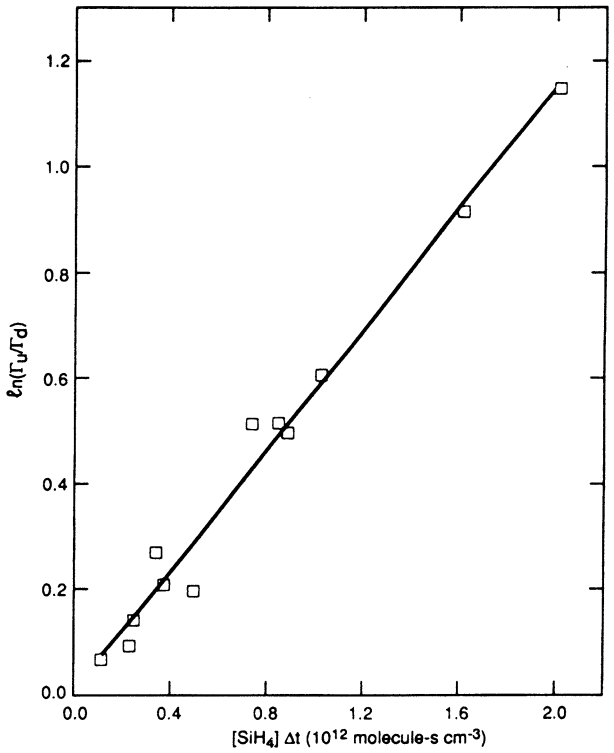

Figure 4. Net quenching of $N_2(X,v\geq 6)$ by silane. The data are derived from the $N_2(A)$ energy transfer diagnostic and are plotted according to eq 16. The slope of the line through the data is the vibrational quenching rate coefficient, k_v.

$$I = k_r[N_2(B)] = \frac{k_3[N_2(X,v'')]_o e^{-k_v[Q]\Delta t}}{1 + \dfrac{k_Q[Q]}{k_r}} \tag{15}$$

where k_v is the rate coefficient for $N_2(X,v'')$ quenching and Δt is the time the quencher and the $N_2(X,v'')$ are mixed. The $N_2(X,v'')$ quenching rate coefficient is determined from the slope of the natural log of the ratio to Stern−Volmer factors at long to short decay times plotted against $[Q]\Delta t$, i.e.,

$$\ln(\Gamma_u/\Gamma_d) = k_v[Q]\Delta t \tag{16}$$

where the subscripts "u" and "d" refer to measurements with the injector in the upstream and downstream positions, respectively.

We should probably mention that $N_2(v)$ (and $SiH_4(v)$) will be quenched in collisions with the reactor walls. This effect is a relatively inefficient process, generally requiring upward of a thousand collisions on average to effect on glass surfaces. Because our observations use a fixed-point technique, such losses are essentially invariant and only provide a constant background decay that has no bearing on our kinetic analyses. As a result, we have ignored them in our kinetic development.

4.2. Results for $N_2(X,v\geq 5)$. Figure 4 shows a representative plot of the data, and Table 1 summarizes all results from the studies using the $N_2(A)$ energy transfer diagnostic. Because rate coefficients for electronic quenching of $N_2(B)$ necessarily are determined in the data analysis, they are also listed in Table 1. The error bars represent one standard deviation of the slopes when data are plotted according to eq 16.

The vibrational relaxation rate coefficients determined by the eq 16 analysis should properly be taken to be lower limits to the true vibrational relaxation rate coefficients. The ν_3 mode of

TABLE 1: Rate Coefficients for $N_2(X,v)$ and $N_2(B^3\Pi_g)$ Quenching by SiH_4

$N_2(X,v)$		$N_2(B,v)$	
vibrational levels	rate coefficient (10^{-13} cm^3 molecule^{-1} s^{-1})	vibrational levels	rate coefficient (10^{-9} cm^3 molecule^{-1} s^{-1})
≥5	4.1 ± 0.5	1	2.2 ±0.5
≥6	5.7 ± 0.3	2	2.7 ± 0.6
≥7	5.3 ± 0.4	3	2.2 ± 0.5
≥8	5.7 ± 0.3	4	2.2 ± 0.7
≥8	5.9 ± 0.4	5	2.8 ± 0.8
≥9	6.0 ± 0.4	6	2.9 ± 0.9
≥10	5.9 ± 0.5	7	2.9 ± 1.2
≥11	5.5 ± 0.6	8	3.4 ± 0.9
≥11	6.4 ± 0.5	9	3.4 ± 0.8
≥12	5.1 ± 0.7	10	4.3 ± 1.3
≥13	5.2 ± 0.8	11	3.0 ± 0.8
≥13	4.9 ± 1.1	12	2.7 ± 1.7
unwtd av	5.5 ± 0.6	unwtd av	2.9 ± 0.6

SiH_4 is resonant to within kT for single quantum transfer from $N_2(X,v)$, so the mechanism for the relaxation most likely proceeds by single-quantum transfer. Some multiquantum transfer, however, is possible as we have found to happen in the $N_2(X,v)/N_2O$ system (vide infra).

With this particular diagnostic there is some uncertainty in the identity of the levels (or level) primarily responsible for exciting the observed $N_2(B,v)$. We can only know for certain that they are above a given v''. Thus the actual process being measured is the net difference in the quenching of the particular levels responsible for the observed $N_2(B,v)$ excitation and the possible repopulation by quenching of higher lying levels which do not themselves contribute to the particular $N_2(B,v)$ being monitored. Even so, the lower-limit vibrational relaxation rate coefficients are quite large, being about twice the size of the rate coefficient for quenching $N_2(X,v)$ by N_2O and an order of magnitude or more greater than the rate coefficients for vibrational relaxation by CO, CO_2, and N_2,[13] species that are generally considered to be effective at removing vibrational energy from $N_2(X,v)$.

The rate coefficients for electronic quenching of $N_2(B)$ seemed unusually large and caused some concern as to the validity of our measurements. Because the primary measurement is of the ratio of two intensities, calibration of the optical system will not contribute to possible errors in the rate coefficients. The other two measured quantities, $[SiH_4]$ and Δt, both depend primarily on gas flow rate measurements. Consequently, we did an extensive set of recalibrations of our flow meters. The results of these new calibrations showed excellent agreement (within 5%) both with previous calibrations and with manufacturer's specifications for a number of different gases and flow meters.

We also considered the effects of $N_2(X,v)$ quenching during the short transit time from the SiH_4 injector to the observation region when the injector was in the downstream position. This correction generally amounted to no more than 10−20% but has been incorporated into the results given in Table 1.

Finally, we note that we have used this same technique to measure rate coefficients for $N_2(B)$ quenching by a variety of other gases with reasonable agreement between our results and those of other groups who used different measurement techniques.[13] It appears, therefore, that silane quenches $N_2(B)$ with remarkable efficiency. The attractive forces between the two molecules are sufficiently strong that quenching takes place at a rate significantly greater than the hard-sphere collision rate.

4.3. Results for $N_2(X,v\leq6)$. An analysis of the variations in the number densities of $N_2(X,v\leq6)$, determined from the He* Penning-ionization diagnostic, as a function of the product

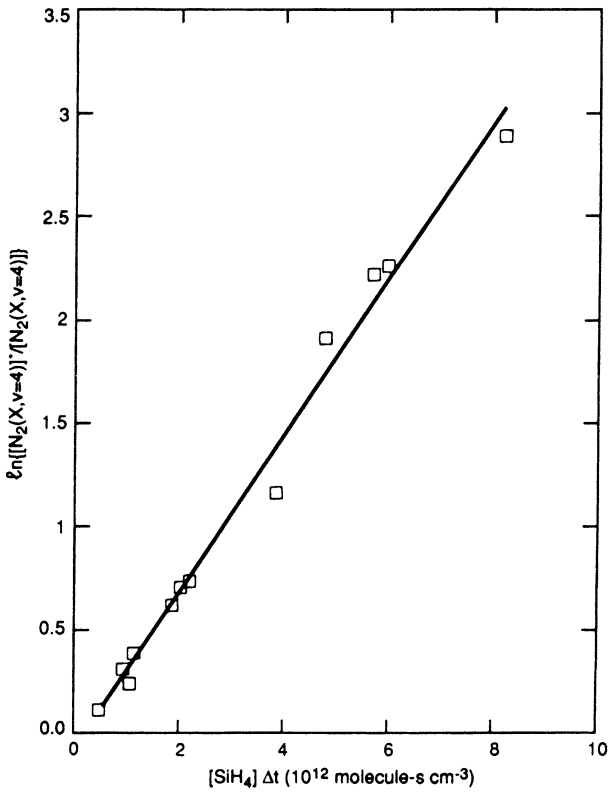

Figure 5. Net quenching of $N_2(X,v=4)$ by SiH_4. The data are derived from the Penning-ionization diagnostic and are plotted according to an analysis similar to eq 16.

TABLE 2: Rate Coefficients for Relaxation of $N_2(X,v)$ Using the Penning-Ionization Diagnostic

	rate coefficient[a]	
vibrational level	net removal	single quantum transfer analysis
1	0.84 ± 0.05	1.3 ± 0.1 1.2[b]
2	1.8 ± 0.1	2.6 ± 0.2
3	2.8 ± 0.1	3.6 ± 0.2
4	3.8 ± 0.1	6.0 ± 1.0
5	4.8 ± 0.2	6.0 ± 1.0
6	5.8 ± 0.2	4.5 ± 1.0

[a] Rate coefficients at 300 K in units of 10^{-13} cm^3 molecule^{-1} s^{-1}. [b] Determined by increase in population of $v'' = 0$.

$[SiH_4]\Delta t$, i.e., equivalent to the analysis related to eq 16, gives plots such as Figure 5 and the set of rate coefficients given in the second column of Table 2. As in the results in Table 1, these values can only properly be considered lower limits.

Because the Penning-ionization diagnostic provides absolute number densities of molecules in each vibrational level, these data are amenable to an alternative analysis that incorporates the effects of single quantum transfer from a given level to the one below it. Although the form of our data set makes the single quantum analysis somewhat crude, the results are still enlightening.

The differential equation describing the time rate of change of molecules in level v with number density N_v is

$$\frac{dN_v}{dt} = k_{v+1}N_{v+1}[SiH_4] - k_vN_v[SiH_4] \qquad (17)$$

where the first term on the right-hand side of the equation represents the rate of formation of level v from level $v + 1$

above, and the second term represents the removal rate from level v into level $v - 1$. Rearranging this equation and integrating it gives

$$\int dN_v = N_v - N_v^o = k_{v+1}[SiH_4] \int N_{v+1}\, dt - k_v[SiH_4] \int N_v\, dt \quad (18)$$

An approximate value for the integral expressions on the right-hand side of eq 18 is

$$\int N_v\, dt \approx \frac{N_v^o + N_v}{2} \Delta t \quad (19)$$

Thus we can rewrite eq 18 as

$$N_v - N_v^o = k_{v+1}\left(\frac{N_{v+1}^o + N_{v+1}}{2}\right)[SiH_4]\Delta t - k_v\left(\frac{N_v^o + N_v}{2}\right)[SiH_4]\Delta t \quad (20)$$

Summing the equation from level v up to level v_{max}, the highest vibrational level observed, gives

$$\sum_v^{v_{max}} (N_v - N_v^o) = k_{v_{max}}\left(\frac{N_{v_{max}}^o + N_{v_{max}}}{2}\right)[SiH_4]\Delta t - k_v\left(\frac{N_v^o + N_v}{2}\right)[SiH_4]\Delta t \quad (21)$$

Because the vibrational population falls off fairly rapidly as v increases, the term in v_{max} can be neglected compared to the term in v, provided v is several quanta below v_{max}. Thus after rearrangement we are left with a simple two-term expression:

$$2\frac{\sum_v^{v_{max}} N_v^o - N_v}{N_v^o + N_v} = k_v[SiH_4]\Delta t \quad (22)$$

What this equation says is that the number of molecules lost from level v is not just that determined from the direct change in the population of level v itself but actually includes the sum of the population lost by all molecules in vibrational levels above v.

Figure 6 shows some of our data plotted according to eq 22. The slope of the line in this plot gives the value of the vibrational relaxation rate coefficient. The rate coefficients for all levels analyzed in this manner are tabulated in the third column of Table 2. The analysis via single quantum transfer gives somewhat larger values for the rate coefficients for relaxation of $v = 1$ and 2 but approaches the values derived from an analysis via eq 16 for higher vibrational levels.

The least-squares fits to the plots related to the eq 22 analysis have near zero intercepts for the lowest vibrational levels, but the intercepts become increasingly larger for the higher vibrational levels. This probably results from neglecting the populations of vibrational levels above 6 in the analysis. As the N_2 vibrational distribution becomes increasingly more quenched, the populations initially in higher levels will cascade down and contribute significantly to the populations of the lower levels. That is, when very little overall quenching has occurred, vibrational levels 7 and above will contribute negligibly to the populations of levels such as 3 or 4. When quenching becomes more significant, however, much of the residual population in levels such as 3 and 4 may well have originated in levels 7 and above. Because the Penning-ionization diagnostic cannot provide information about the populations of these higher levels, our analysis necessarily excludes them from consideration. Were it possible to include them, the ordinates of the points at the larger values of $[SiH_4]\Delta t$ would undoubtedly be higher. This effect would both increase the slope, thus increasing the rate coefficient, and also would lower the intercept, indicating that a sufficiently large set of vibrational levels had been included in the analysis.

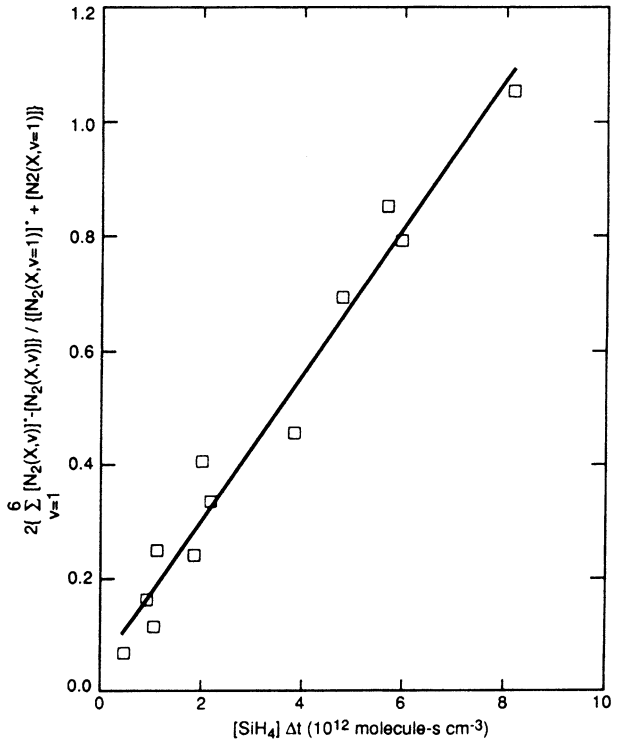

Figure 6. Single quantum analysis of quenching of $N_2(X,v=1)$ by SiH_4. The data are derived from the Penning-ionization diagnostic and are plotted according to eq 22.

The rate coefficient for relaxing vibrational level 1 can also be determined from an analysis of the increase in population of vibrational level 0. In this case the analysis equation is

$$2\frac{N_0 - N_0^o}{N_1 + N_1^o} = k_{v=1}[SiH_4]\Delta t \quad (23)$$

This equation results because $v = 0$ has no loss processes, and because in single quantum transfer, only those molecules removed from $v = 1$ can enter $v = 0$. Figure 7 shows the data plot relevant to eq 23. The rate coefficient determined from these data is 1.2×10^{-13} cm^3 molecule^{-1} s^{-1}, in excellent agreement with the value determined by considering the decay of $v = 1$.

5. $SiH_4(\nu_3)$ Excitation by $N_2(X,v)$

We used the apparatus shown in Figure 2 to investigate the excitation of $SiH_4(\nu_3)$ by vibration−vibration transfer from $N_2(X,v)$ to SiH_4. Because the ν_3 mode of SiH_4 is resonant within kT with single quantum transfer from all $N_2(X,v \leq 15)$, ν_3 excitation seemed the most logical choice for the efficient quenching reaction. The ν_3 mode fundamental frequency is 2190 cm^{-1} (4570 nm) and its band strength is 625 cm^{-2} atm^{-1} at

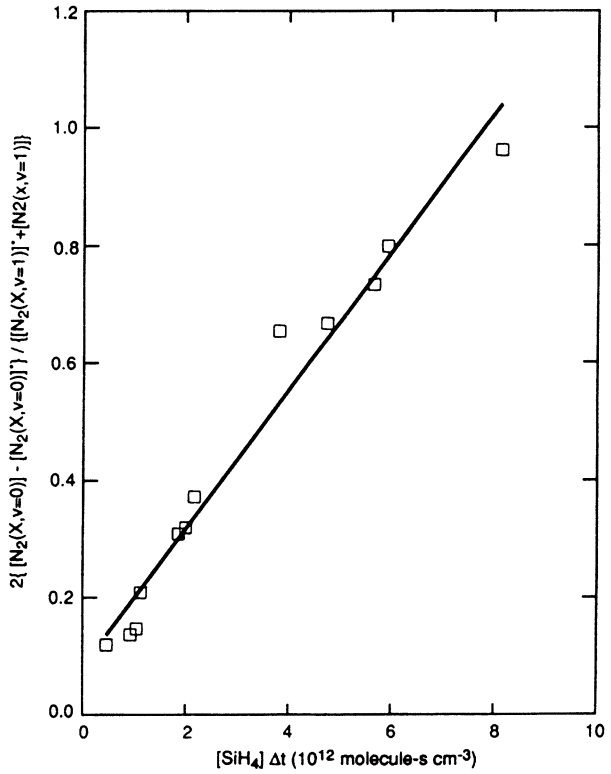

Figure 7. Analysis of the quenching of $N_2(X,v=1)$ by SiH_4 from observations of the increase in $[N_2(X,v=0)]$ as a function of $[SiH_4]$. The data are plotted according to eq 23.

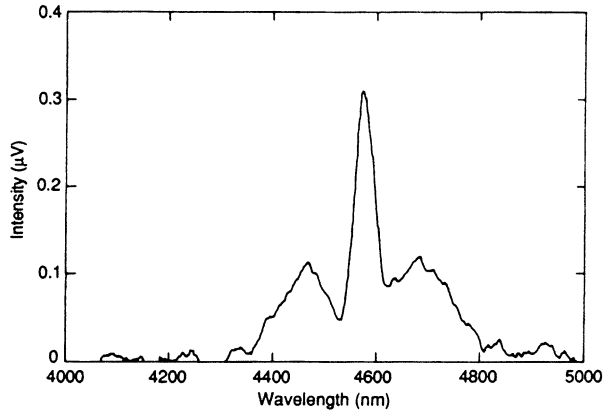

Figure 8. Spectrum of $SiH_4(\nu_3)$ emission excited by $N_2(v)$.

STP.[34] We compared our observations with observations $N_2O(\nu_3)$ excitation by $N_2(X,v)$ when N_2O was added to the reactor. The N_2O ν_3 mode radiates at 2224 cm^{-1} (4500 nm) and its band strength is 1541 cm^{-2} atm^{-1} at STP.[35]

Figure 8 shows the fluorescence spectrum between 4 and 5 μm when SiH_4 is added to a flow of $N_2(X,v)$. The strong Q-branch of the SiH_4 ν_3 mode is visible at 4.58 μm with associated P and R ranches to either side. The spectral resolution is 0.04 μm, and the SiH_4 number density is about 1.5×10^{14} molecules cm^{-3}. For comparison, Figure 9 shows the fluorescence spectrum excited when N_2O is added to $N_2(X,v)$. Here the spectral resolution is 0.01 μm and the N_2O number density is about 5×10^{13} molecules cm^{-3}. In addition to the $N_2O(\nu_3)$ fundamental band centered at 4.50 μm, N_2O hot-band emission is evident from $\nu_3 = 2$ at 4.56 μm and $\nu_3 = 3$ at 4.62 μm. This demonstrates, that in the case of N_2O quenching at least, multiquantum vibrational energy transfer is likely.

Figure 10 shows how the emission from $SiH_4(\nu_3)$ at 4.56 μm varies as a function of SiH_4 number density added to the reactor.

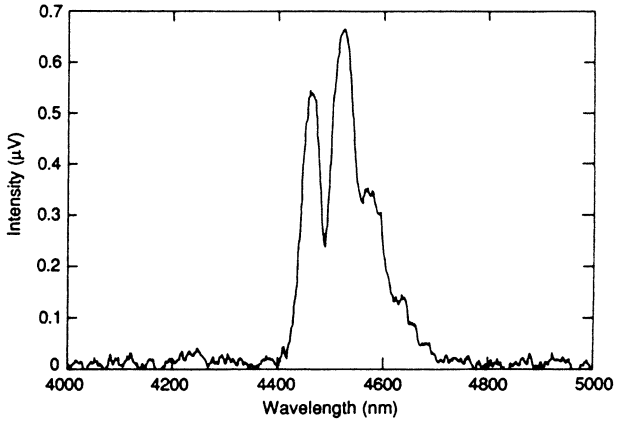

Figure 9. Spectrum of $N_2O(\nu_3)$ emission excited by $N_2(v)$.

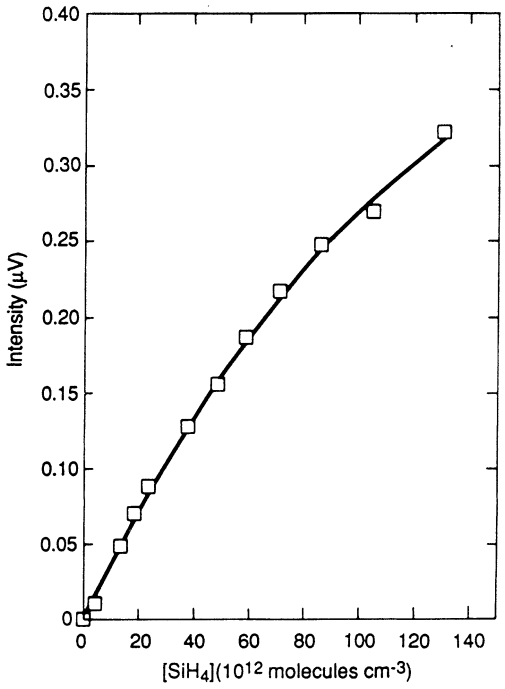

Figure 10. Intensity of $SiH_4(\nu_3)$ emission as a function of $[SiH_4]$ added to $N_2(X,v)$. The solid line is a least-squares fit to eq 32 with $k_{24} = 2.5 \times 10^{-13}$ cm^3 $molecule^{-1}$ s^{-1} and $k_{25} = 28$ s^{-1}.

At low number densities, the emission intensity increases almost linearly with increases in SiH_4 number density. For higher SiH_4 additions, however, the emission intensity increase is less than linear. Two different effects are responsible for this decrease in linearity. The higher SiH_4 number densities reduce the effective $N_2(X,v)$ number density in the detector's field of view, thereby lowering the rate of $SiH_4(\nu_3)$ excitation. In addition, higher number densities of added SiH_4 quench the SiH_4 emission. We can test these suppositions with a simple kinetic model.

We base this model upon the following set of reactions:

$$SiH_4 + N_2(X,v) \rightarrow SiH_4(w) + N_2(X,v-1) \quad (24a)$$

$$\rightarrow \text{other products} \quad (24b)$$

$$SiH_4(w) \rightarrow SiH_4 + h\nu \quad (25)$$

$$SiH_4(w) + SiH_4 \rightarrow 2SiH_4 \quad (26)$$

$$SiH_4(w) + Ar, N_2 \rightarrow SiH_4 + Ar, N_2 \quad (27)$$

Although reaction 27, bath-gas quenching, could not be deduced

from the data in Figure 10, the necessity for its inclusion becomes apparent when $SiH_4^\dagger$ excitation is studied at several different pressures.

With the above reaction scheme, we can write down and solve two differential equations describing the temporal variations in the number densities of $N_2(X,v)$ and $SiH_4(w)$. For $N_2(X,v)$ we have

$$\frac{d[N_2(X,v)]}{dt} = -k_{24}[SiH_4][N_2(X,v)] \quad (28)$$

This equation can be solved to give

$$[N_2(X,v)] = [N_2(X,v)]_o \exp(-k_{24}[SiH_4]t) \quad (29)$$

where $[N_2(X,v)]_o$ is the $N_2(X,v)$ number density in the absence of SiH_4. For $SiH_4(w)$ we have

$$\frac{d[SiH_4(w)]}{dt} = k_{24a}[SiH_4][N_2(X,v)] - (k_{25} + k_{26}[SiH_4] + k_{27}[Ar,N_2])[SiH_4(w)] \quad (30)$$

Using eq 29 for $[N_2(X,v)]$, eq 30 can be solved to give

$$[SiH_4(w)] = \{[k_{24a}[N_2(X,v)]_o[SiH_4](\exp(-k_{24}[SiH_4]t) - \exp(-(k_{25} + k_{26}[SiH_4] + k_{27}[Ar,N_2])t))]/ [k_{25} + k_{26}[SiH_4] + k_{27}[Ar,N_2] - k_{24}[SiH_4]]\} \quad (31)$$

Because we are looking along the axis of the flow reactor, our effective field of view encompasses emissions from volume elements at all axial positions, and thereby reaction times, between zero and the bend in the flow reactor, 36 cm distant from the SiH_4 injector. Thus the observed emission is in reality the integral over time of emission from each of these volume elements. The product of the collection efficiency times the area of each volume element normal to the flow tube axis is constant until the monochromator field of view becomes comparable to the cross-sectional area of the flow tube. This happens in our reactor about 24 cm downstream from the injector. Over the last 12 cm of the field of view, the product of collection efficiency times volume decreases slowly so that at the farthest reaches of the flow reactor, the effective photon emission rates are attenuated by almost a factor of 2 compared to those arising from emission in the first 24 cm of the reactor. Rather than account for this effect exactly, we found it convenient to correct our observations by assuming constant collection efficiency over a column shorter than actually observed. This allows for easier integration of eq 31 over time and has a negligible effect on the results.

The observed emission intensity is then the product of k_{25} times the integrated number density of $SiH_4(w)$ along the length of the observation volume:

$$I = \frac{\varsigma k_{24a}k_{25}[N_2(X,v)]_o[SiH_4]}{k_{25} + k_{26}[SiH_4] + k_{27}[Ar,N_2] - k_{24}[SiH_4]} \times \left\{\frac{(1 - \exp(-k_{24}[SiH_4]t_o))}{k_{24}[SiH_4]} - \frac{(1 - \exp(-(k_{25} + k_{26}[SiH_4] + k_{27}[Ar,N_2])t_o))}{(k_{25} + k_{26}[SiH_4] + k_{27}[Ar,N_2])}\right\} \quad (32)$$

where t_o is the effective time along the length of the observation region and the factor ς is an efficiency factor for the detection system.

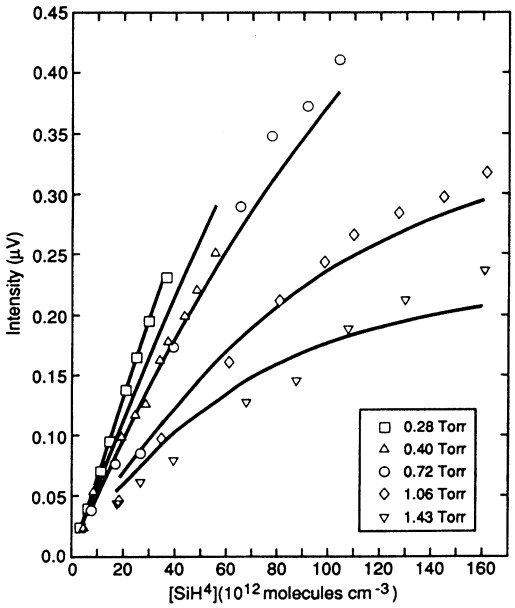

Figure 11. Excitation of $SiH_4(\nu_3)$ by $N_2(X,v)$ at various total argon pressures compared to a kinetic model based on eq 32.

We subjected the data in Figure 10 to a least-squares analysis according to eq 32 with the unknown parameters being the product $\zeta k_{24a}k_{25}[N_2(X,v)]_o$ and k_{26}. We determined a value for k_{24} from our earlier work to be between 1×10^{-13} and 5.5×10^{-13} cm^3 molecule^{-1} s^{-1}, depending upon vibrational level, and k_{25} can be calculated from the measured SiH_4 ν_3 band strength. Given a band strength of 625 cm^{-2} atm^{-1}, we calculate a radiative decay rate of 28 s^{-1} for the triply degenerate $SiH_4(\nu_3)$. The results of the least-squares fit, for an assumed value $k_{24} = 2.5 \times 10^{-13}$ cm^3 molecule^{-1} s^{-1}, are 3.1×10^{-11} for the product $\zeta k_{24a}k_{25}[N_2(X,v)]_o$ and 4.5×10^{-13} cm^3 molecule^1 s^{-1} for k_{26}. The solid line in Figure 10 compares the results of the fit to the data. These results show that SiH_4 self-quenching (reaction 26) is quite efficient.

To compare with the SiH_4 excitation data, we studied the excitation of $N_2O(\nu_3)$ under identical conditions. This affords comparison of the relative excitation efficiencies between the two reactions. A set of equations analagous to eqs 24−32 also holds for the N_2O data analysis. When necessary, we prime the k's for the rate coefficients for the N_2O reactions to distinguish them from those for the SiH_4 reactions.

Data taken at several different pressures are shown in Figure 11 for SiH_4 excitation and, for comparison purposes, Figure 12 for N_2O excitation. It is clear from the way the initial slopes of the SiH_4 data become much smaller for the higher pressure data, in contrast to the near constancy for the N_2O data, that bath gas quenching of $SiH_4(\nu_3)$ is fairly significant. The variations in the initial slopes can result from the effects of reaction 27 or 27′ or from changes in $[N_2(X,v)]_o$. Because at each pressure the value of $[N_2(X,v)]_o$ will be the same for both sets of data, we should be able to analyze the data to allow estimation of k_{27}. In addition, by comparing the observed intensities, we should be able to determine a ratio of k_{24a}/k_{24a}'. Values for k_{24}, k_{24}' and k_{25}, k_{25}' can be estimated from the known quenching data and band strength measurements, respectively. The band strength data give values of k_{25} and k_{25}' of 28 and 214 s^{-1}, respectively, whereas our quenching data indicate a value for k_{24} and k_{24}' of about 2.5×10^{-13} and 1×10^{-13} cm^3 molecule^{-1} s^{-1}, respectively. For the two parameters we can determine from the data of Figures 11 and 12, the actual values used for k_{24} and k_{24}' are not particularly important. Variations in both

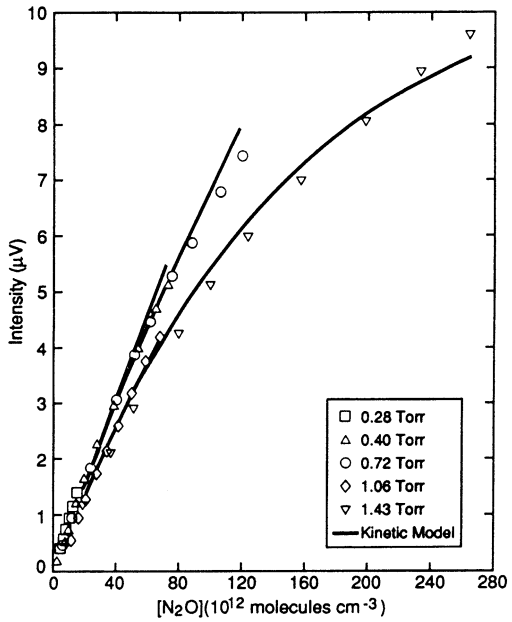

Figure 12. Excitation of $N_2O(\nu_3)$ by $N_2(X,v)$ at various total pressures of argon compared to a kinetic model based on eq 32.

quantities of 30−50% give similar results for k_{27} and for the ratio k_{24a}/k_{24a}'. The particular values chosen for k_{26}, k_{26}', and k_{27}' can be varied almost at will without affecting the final results for the quantities k_{24a}/k_{24a}' and k_{27}. Our results indicate the ratio k_{24a}/k_{24a}' is 0.35 ± 0.05 and k_{27} is $(6 \pm 2) \times 10^{-15}$ cm^3 molecule^{-1} s^{-1}.

Given that the ratio k_{24}/k_{24}' is about 2.5, the result above indicates that $N_2(X,v)$ energy transfer to N_2O is about 7 times more efficient at producing infrared radiation at 4500 nm than is energy transfer to SiH_4. Put another way, if the branching ratio, k_{24a}'/k_{24}' is unity, then only about 15% of the time will an $N_2(X,v)$ quantum transferred to SiH_4 appear as radiation at 4500 nm. One reason for this discrepancy is undoubtedly related to the fact that SiH_4 has an infrared inactive vibrational mode, ν_1, that is also resonant with $N_2(X,v)$ single-quantum transfer. Evidence for excitation of this band could appear in the infrared in a combination band. Although we searched the region between 2000 and 5000 nm, we saw no other emissions that we could ascribe to SiH_4 infrared radiation. Our system is not particularly sensitive, however, and these bands are likely to be much weaker than the ν_3 band.

6. Summarizing Remarks

We have shown how several different diagnostics for $N_2(X,v)$ that we developed previously can be used in kinetic studies involving the transfer of vibrational energy from $N_2(X,v)$ in such a manner as to allow individual energy-transfer rate coefficients to be determined for a number of specific vibrational levels. In the case of vibrational levels below $v'' = 6$, the state specificity is exact and one can make one-to-one correlations between the diagnostic and $N_2(X,v)$ levels. For higher vibrational levels, up to at least $v'' = 13$, one can make measurements that are valid only for levels above a given v''. We cannot know, however, which specific levels (or level) above v'' are primarily responsible for the observed effects.

In this particular study, we used silane for the energy transfer partner because of the probable importance of the $N_2(X,v)$ plus silane reaction, reaction 1, in initiating silane decomposition in silicon nitride coating systems using the RPECVD technique. We find that silane quenches vibrational energy from $N_2(X,v)$ very rapidly. The vibrational energy transfer rate coefficients vary from about 1×10^{-13} cm^3 molecule^{-1} s^{-1} for $v'' = 0$ up to about 6×10^{-13} cm^3 molecule^{-1} s^{-1} for $v'' > 4$ and up to 13. For the low vibrational levels, analysis using a single-quantum transfer model gives results consistent with total removal rate coefficient measurements. In addition, under the assumptions involved in the single-quantum transfer model, the rate coefficient for removal of $v'' = 1$ is the same as that for the increase in $v'' = 0$.

Observations in the infrared show that one major channel for the energy transfer involves $SiH_4(\nu_3)$ excitation. The data have been analyzed to indicate an energy transfer rate coefficient, in this case nonstate specific, of about 2.5×10^{-13} cm^3 molecule^{-1} s^{-1}. This value is consistent with the other measurements given that the bulk of the $N_2(X,v)$ population will be in the lowest vibrational levels. In addition, comparison of $SiH_4(\nu_3)$ emission intensities with those from $N_2O(\nu_3)$ excitation by $N_2(X,v)$ indicate that only about 15% of quenching events result in $SiH_4(\nu_3)$ excitation.

By way of comparison, we note that rate coefficients for molecules considered to be efficient quenchers $N_2(X,v)$ vibrational energy are generally smaller than those measured in this study. That is the rate coefficients for the $N_2(X,v)/N_2O$ interaction are about 1×10^{-13} cm^3 molecule^{-1} s^{-1} for unspecified, but primarily lower, vibrational levels[1,2] and 3×10^{-13} cm^3 molecule^{-1} s^{-1} for higher vibrational levels.[5] In the case of the $N_2(X,v)/CO_2$ interaction, published rate coefficients vary between 0.8×10^{-13} and 2×10^{-13} cm^3 molecule^{-1} s^{-1} for unspecified, but primarily lower, vibrational levels[1,2] and 0.4×10^{-13} cm^3 molecule^{-1} s^{-1} for higher vibrational levels.[5] Even in the case of $N_2(v)$ quenching by H_2O, the rate coefficient is considerably smaller, 1.2×10^{-14} cm^3 molecule^{-1} s^{-1} for $v'' = 1$.[4]

Acknowledgment. We appreciate partial financial support of this work by the Aero Propulsion and Power Directorate of the Wright Laboratory under contract F33615−91-C-2112.

References and Notes

(1) Morgan, J. E.; Schiff, H. I. *Can. J. Chem.* **1963**, *41*, 903.
(2) McNeal, R. J.; Whitson, M. E., Jr.; Cook, G. R. *J. Chem. Phys.* **1972**, *57*, 4752.
(3) McNeal, R. J.; Whitson, M. E., Jr.; Cook, G. R. *J. Geophys Res.* **1974**, *79*, 1527.
(4) Whitson, M. E., Jr.; McNeal, R. J. *J. Chem. Phys.* **1977**, *66*, 2696.
(5) Starr, W. L.; Shaw, T. M. *J. Chem. Phys.* **1966**, *44*, 4181.
(6) De Benedictis, S.; Capitelli, M.; Cramarossa, F.; Gorse, C. *Chem. Phys.* **1987**, *111*, 361.
(7) Mutel, B.; Dessaux, O.; Goudmand, P.; Bridoux, M.; Dupret, C. *J. Quant. Spectrosc. Radiat. Transfer* **1986**, *35*, 23.
(8) Devyatov, A. A.; Dolenko, S. A.; Rahkimov, A. T.; Rakhimova, T. V.; Roi, N. N.; Suetin, N. V. *Sov. Phys.-JETP* **1986**, *63*, 246.
(9) Vereshchagin, K. A.; Smirnov, V. V.; Shakhatov, V. A. *Int. Conference on Phenom. in Ionized Gases, XXIII* **1997**, *1*, 42.
(10) Piper, L. G.; Donohue, K.; Kessler, W. J.; Tucker, T. R.; Cummings, W. P.; Marinelli, W. J.; Davis, S. J. Laser-Based Diagnostics for $N_2(X,v)$. PSI-TR-960, Final Report to the Air Force Weapons Laboratory under Contract No. F29601-87-C-0056, 1990. Also published by the Weapons Laboratory (AFSC) as WL-TR-90−45. Available from NTIS, ADA229310.
(11) Piper, L. G. *J. Chem. Phys.* **1989**, *91*, 864.
(12) Piper, L. G. *J. Chem. Phys.* **1994**, *101*, 10229.
(13) Piper, L. G. *J. Chem. Phys.* **1992**, *97*, 270.
(14) Schmeltekopf, A. L.; Ferguson, E. E.; Fehsenfeld, F. C. *J. Chem. Phys.* **1968**, *48*, 966.
(15) Young, S. J.; Horn, K. P. *J. Chem. Phys.* **1972**, *57*, 4835.
(16) Young, S. J. *J. Chem. Phys.* **1973**, *38*, 1603.
(17) Piper, L. G.; Marinelli, W. J. *J. Chem. Phys.* **1988**, *89*, 2918.
(18) Lucovsky, G.; Richard, P. D.; Tsu, D. V.; Lin, S. Y.; Markunas, R. J. *J. Vac. Sci. Technol.* **1986**, *A4*, 681.

(19) Lauinger, T.; Moschner, J.; Aberle, A. G.; Hezel, R. *J. Vac. Sci. Technol* A **1998**, *16*, 530.
(20) Alexandrov, S. E.; Kovalgin, A. Yu. *Adv. Mater. Opt. Electron*. **1998**, *8*, 13.
(21) Alexandrov, S. E.; Hitchman, M. L.; Kovalgin, A. Yu. *Adv. Mater. Opt. Electron*. **1998**, *8*, 23.
(22) Park, Y.-B.; Rhee, S.-W. *J. Mater. Sci., Mater. Electron*. **2001**, *12*, 515.
(23) DeJoseph, C. A. Reactions of Silane in active nitrogen. WRDC-TR-90-2001, Final Report, 1990. Available from NTIS, ADA220371.
(24) Piper, L. G. *J. Phys. Chem.* **1991**, *95*, 3965.
(25) Stedman, D. H.; Setser, D. W. *Chem. Phys. Lett.* **1968**, *2*, 542.
(26) Piper, L. G.; Gundel, L.; Velazco, J. E.; Setser, D. W. *J. Chem. Phys.* **1975**, *62*, 3883.
(27) Piper, L. G.; Holtzclaw, K. W.; Green, B. D.; Blumberg, W. A. M. *J. Chem. Phys.* **1989**, *90*, 5337.
(28) Piper, L. G.; Davis, S. J.; Murphy, H. C.; Cummings, W. C.; Walkauskas, L. P.; DeFaccio, M. A.; Cowles, L. M.; Rawlins, W. T.; Marinelli, W. J.; Green, B. D. CONAN: Chemistry of Nitrogen-A Nascence. Final Technical Report PSI-076/TR-593 for the period 4 September 1984 through 4 June 1986 under Contract No. F29601-84-C-0076, January 1987. Also published by the Weapons Laboratory (AFSC) as AFWL-TR-86-95. Available from NTIS, ADA193122.
(29) Treanor, C. E.; Rich, J. W.; Rehm, R. G. *J. Chem. Phys.* **1968**, *43*, 1798.
(30) Caledonia, G. E.; Center, R. E. *J. Chem. Phys.* **1971**, *55*, 552.
(31) Dilonardo, M.; Capitelli, M. *Rev. Phys. Appl.* **1978**, *13*, 115.
(32) Davis, S. J.; Piper, L. G. *J. Phys. Chem.* **1990**, *94*, 4515.
(33) Stern, O.; Volmer, M. *Phys. Z.* **1919**, *20*, 183.
(34) Allen, W. D.; Schaefer, H. F., III. *Chem. Phys.* **1986**, *108*, 243.
(35) Kagan, R. H. *J. Mol. Spectrosc.* **1982**, *95*, 297.